



Advanced design of integrated vibration control systems for adjacent buildings under seismic excitations

Francisco Palacios-Quinonero¹, Josep Rubió-Massegú¹, Josep M Rossell¹ and Hamid Reza Karimi²

¹CoDaLab, Department of Mathematics, Universitat Politècnica de Catalunya (UPC), Av. Bases de Manresa 61–73, 08242 Manresa, Barcelona, Spain

²Politecnico di Milano, Department of Mechanical Engineering, via La Masa 1, 20156 Milan, Italy

E-mail: {francisco.palacios,josep.rubio,josep.maria.rossell}@upc.edu, hamidreza.karimi@polimi.it

Abstract. In vibration control of adjacent buildings under seismic excitations, a twofold objective has to be considered: (i) to mitigate the vibrational response of the individual structures and (ii) to provide a suitable protection against interbuilding impacts (pounding). An interesting strategy to deal with this complex control problem consists in considering an integrated control system, which combines interbuilding actuation devices with local control systems implemented in the individual buildings. In this paper, an effective computational strategy to design this kind of integrated control systems is presented. The proposed design methodology is based on a linear matrix inequality formulation, allows including active and passive actuation devices, and makes it possible to deal with important information constraints associated to the problem. The main ideas are illustrated by means of a two-building system equipped with three actuation devices: two interstory actuation devices implemented at the ground level of the buildings, plus an interbuilding actuation device installed at the top level of the lowest building. For this control setup, two different integrated controllers are designed. A proper set of numerical simulations is conducted to assess the performance of the proposed controllers with positive results.

1. Introduction

In control systems for seismic protection of closely adjacent buildings two different elements need to be considered. Firstly, the structural vibrational response of the individual buildings that should be mitigated to avoid structural damage. Secondly, the interbuilding collisions (pounding), which should also be prevented to avoid the damaging effects associated to massive pounding impacts [1–3]. Likewise, two different kinds of actuation devices can be considered in this context. On one hand, *inbuilding actuators*, which are implemented in a particular building and exert structural forces restricted to this building. On the other hand, *interbuilding actuators* that are implemented between adjacent buildings and produce structural forces affecting both buildings. The idea of using interbuilding actuation devices for vibration control of adjacent buildings has been used in several papers with positive results (see for example [4–10]). However, all these works are only focused on mitigating the vibrational response of the individual

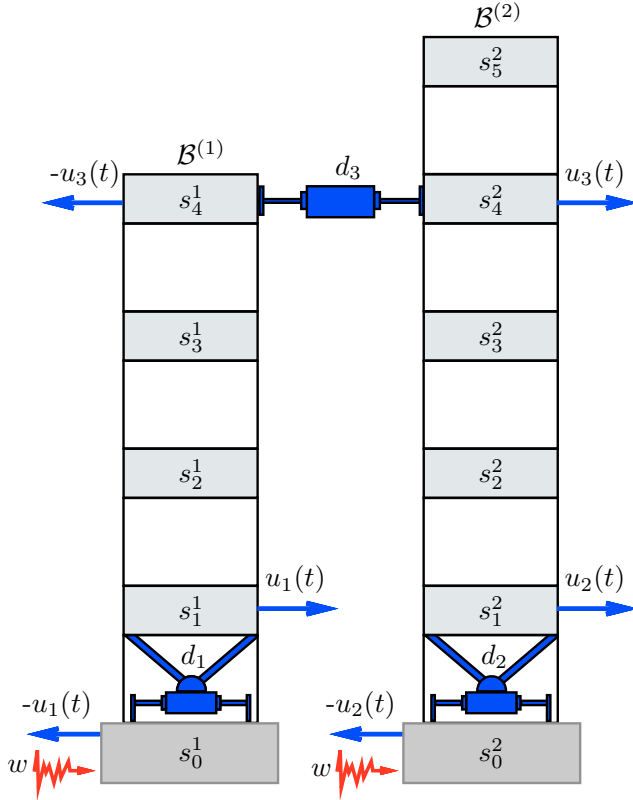


Figure 1. Two-building system equipped with two interstory actuation devices (d_1 and d_2) and an interbuilding actuator (d_3).

buildings. A broader formulation is presented in [11–13], where *interstory drifts* and *interbuilding approaches* are considered to describe the overall vibrational response of adjacent buildings.

The objective of this paper is the presentation of an advanced controller design strategy for seismic protection of adjacent buildings. This strategy is based on a linear matrix inequality (LMI) formulation and facilitates the integrated design of control systems with inbuilding and interbuilding actuation devices. Additionally, it also allows dealing with the natural information constraints associated to the problem. The main ideas are introduced by means of a particular two-building system formed by a four-story building adjacent to a five-story building and equipped with three actuation devices (see Figure 1). For this control setup, two static output-feedback H_∞ controllers are designed: (i) a centralized velocity-feedback active controller and (ii) a fully decentralized velocity-feedback controller, which can be implemented using passive linear dampers. To assess the effectiveness of the proposed controllers, numerical simulations are conducted using the full scale North–South El Centro 1940 seismic record as ground acceleration disturbance.

The rest of the paper is organized as follows: In Section 2, a state-space model for the two-building system is provided. In Section 3, the static output-feedback H_∞ controllers are designed. In Section 4, a proper set of numerical simulations are conducted to assess the controllers' performance. Finally, some conclusions and future research directions are presented in Section 5.

2. Two-building system model

Let us consider a two-building system formed by a four-story building adjacent to a five-story building as schematically depicted in Figure 1. The buildings' lateral motion can be described by the following second-order differential equation:

$$\mathbf{M}\ddot{\mathbf{q}}(t) + \mathbf{C}_d\dot{\mathbf{q}}(t) + \mathbf{K}_s\mathbf{q}(t) = \mathbf{T}_u\mathbf{u}(t) + \mathbf{T}_w w(t), \quad (1)$$

where \mathbf{M} is the mass matrix, \mathbf{C}_d is the damping matrix and \mathbf{K}_s is the stiffness matrix. The story displacements with respect to the ground are collected in the vector

$$\mathbf{q}(t) = \begin{bmatrix} \mathbf{q}^{(1)}(t) \\ \mathbf{q}^{(2)}(t) \end{bmatrix}, \quad (2)$$

where

$$\mathbf{q}^{(1)}(t) = [q_1^1(t), q_2^1(t), q_3^1(t), q_4^1(t)]^T, \quad \mathbf{q}^{(2)}(t) = [q_1^2(t), q_2^2(t), q_3^2(t), q_4^2(t), q_5^2(t)]^T, \quad (3)$$

and $q_i^j(t)$ represents the displacement of the i th story in the building $\mathcal{B}^{(j)}$ (denoted as s_i^j in Figure 1) with respect to the building's ground level s_0^j . The system incorporates three force actuation devices: two interstory actuators (d_1 and d_2) located at the buildings' first-story level plus an interbuilding actuator implemented at the fourth-story level (d_3). The vector of control forces is

$$\mathbf{u}(t) = [u_1(t), u_2(t), u_3(t)]^T, \quad (4)$$

where u_i is the control force delivered by the actuation device d_i , which produces a pair of opposite structural forces as indicated in Figure 1. This actuation scheme is modeled by means of the control location matrix \mathbf{T}_u . The ground acceleration disturbance is denoted by $w(t)$, and \mathbf{T}_w is the disturbance input matrix. The mass matrix has the following block diagonal structure:

$$\mathbf{M} = \begin{bmatrix} \mathbf{M}^{(1)} & [\mathbf{0}]_{4 \times 5} \\ [\mathbf{0}]_{5 \times 4} & \mathbf{M}^{(2)} \end{bmatrix}, \quad (5)$$

where $[\mathbf{0}]_{r \times s}$ is a zero matrix of dimensions $r \times s$,

$$\mathbf{M}^{(1)} = \begin{bmatrix} m_1^1 & 0 & 0 & 0 \\ 0 & m_2^1 & 0 & 0 \\ 0 & 0 & m_3^1 & 0 \\ 0 & 0 & 0 & m_4^1 \end{bmatrix}, \quad \mathbf{M}^{(2)} = \begin{bmatrix} m_1^2 & 0 & 0 & 0 & 0 \\ 0 & m_2^2 & 0 & 0 & 0 \\ 0 & 0 & m_3^2 & 0 & 0 \\ 0 & 0 & 0 & m_4^2 & 0 \\ 0 & 0 & 0 & 0 & m_5^2 \end{bmatrix} \quad (6)$$

and m_i^j denotes the mass of the i th story in the building $\mathcal{B}^{(j)}$. The stiffness matrix has the form

$$\mathbf{K}_s = \begin{bmatrix} \mathbf{K}_s^{(1)} & [\mathbf{0}]_{4 \times 5} \\ [\mathbf{0}]_{5 \times 4} & \mathbf{K}_s^{(2)} \end{bmatrix}, \quad (7)$$

where

$$\mathbf{K}_s^{(1)} = \begin{bmatrix} k_1^1 + k_2^1 & -k_2^1 & 0 & 0 \\ -k_2^1 & k_2^1 + k_3^1 & -k_3^1 & 0 \\ 0 & -k_3^1 & k_3^1 + k_4^1 & -k_4^1 \\ 0 & 0 & -k_4^1 & k_4^1 \end{bmatrix}, \quad \mathbf{K}_s^{(2)} = \begin{bmatrix} k_1^2 + k_2^2 & -k_2^2 & 0 & 0 & 0 \\ -k_2^2 & k_2^2 + k_3^2 & -k_3^2 & 0 & 0 \\ 0 & -k_3^2 & k_3^2 + k_4^2 & -k_4^2 & 0 \\ 0 & 0 & -k_4^2 & k_4^2 + k_5^2 & -k_5^2 \\ 0 & 0 & 0 & -k_5^2 & k_5^2 \end{bmatrix} \quad (8)$$

and k_i^j denotes the stiffness coefficient of the i th story in the building $\mathcal{B}^{(j)}$. The damping matrix also has a block diagonal structure of the form

$$\mathbf{C}_d = \begin{bmatrix} \mathbf{C}_d^{(1)} & [\mathbf{0}]_{4 \times 5} \\ [\mathbf{0}]_{5 \times 4} & \mathbf{C}_d^{(2)} \end{bmatrix}. \quad (9)$$

Table 1. Mass and stiffness coefficient values

story	building $\mathcal{B}^{(1)}$					building $\mathcal{B}^{(2)}$				
	1	2	3	4		1	2	3	4	5
mass ($\times 10^5$ Kg)	2.152	2.092	2.070	2.661		2.152	2.092	2.070	2.048	2.661
stiffness ($\times 10^8$ N/m)	1.470	1.130	0.990	0.840		1.470	1.130	0.990	0.890	0.840

where $\mathbf{C}_d^{(j)}$ denotes the damping matrix corresponding to the building $\mathcal{B}^{(j)}$. When the damping coefficients are known, the buildings' damping matrices can be obtained by replacing the stiffness coefficients k_i^j in Eq. (8) by the corresponding damping coefficients c_i^j . However, in most practical situations, the values of the damping coefficients cannot be properly determined and other computational methods are used to obtain the matrices $\mathbf{C}_d^{(j)}$ [14]. The control location matrix and the disturbance input matrix have, respectively, the following form:

$$\mathbf{T}_u = \begin{bmatrix} 1 & 0 & 0 \\ 0 & 0 & 0 \\ 0 & 0 & 0 \\ 0 & 0 & -1 \\ 0 & 1 & 0 \\ 0 & 0 & 0 \\ 0 & 0 & 0 \\ 0 & 0 & 1 \\ 0 & 0 & 0 \end{bmatrix}, \quad \mathbf{T}_w = -\mathbf{M} \begin{bmatrix} 1 \\ 1 \\ 1 \\ 1 \\ 1 \\ 1 \\ 1 \\ 1 \\ 1 \end{bmatrix}. \quad (10)$$

In the controller designs and numerical simulations presented in this paper, the particular values of mass and stiffness coefficients given in Table 1 have been used. These values are similar to those corresponding to the five-story building presented in [15]. The damping matrices $\mathbf{C}_d^{(1)}$ and $\mathbf{C}_d^{(2)}$ have been computed as Rayleigh damping matrices by setting a 2% of relative damping on the corresponding first and last modes. The obtained particular values (in Ns/m) are the following:

$$\mathbf{C}_d^{(1)} = 10^5 \times \begin{bmatrix} 2.6450 & -0.9034 & 0 & 0 \\ -0.9034 & 2.2455 & -0.7915 & 0 \\ 0 & -0.7915 & 2.0078 & -0.6715 \\ 0 & 0 & -0.6715 & 1.3719 \end{bmatrix}, \quad (11)$$

$$\mathbf{C}_d^{(2)} = 10^5 \times \begin{bmatrix} 2.6017 & -0.9244 & 0 & 0 & 0 \\ -0.9244 & 2.1958 & -0.8099 & 0 & 0 \\ 0 & -0.8099 & 1.9946 & -0.7281 & 0 \\ 0 & 0 & -0.7281 & 1.8670 & -0.6872 \\ 0 & 0 & 0 & -0.6872 & 1.2741 \end{bmatrix}. \quad (12)$$

Next, by introducing the augmented state vector

$$\mathbf{x}(t) = \begin{bmatrix} \mathbf{q}(t) \\ \dot{\mathbf{q}}(t) \end{bmatrix}, \quad (13)$$

we obtain a first-order state-space model

$$\dot{\mathbf{x}}(t) = \mathbf{A} \mathbf{x}(t) + \mathbf{B} \mathbf{u}(t) + \mathbf{E} w(t), \quad (14)$$

with the system matrix

$$\mathbf{A} = \begin{bmatrix} [\mathbf{0}]_{9 \times 9} & \mathbf{I}_9 \\ -\mathbf{M}^{-1}\mathbf{K} & -\mathbf{M}^{-1}\mathbf{C} \end{bmatrix} \quad (15)$$

and the following control and disturbance input matrices

$$\mathbf{B} = \begin{bmatrix} [\mathbf{0}]_{9 \times 1} \\ \mathbf{M}^{-1}\mathbf{T}_u \end{bmatrix}, \quad \mathbf{E} = \begin{bmatrix} [\mathbf{0}]_{9 \times 1} \\ -[\mathbf{1}]_{9 \times 1} \end{bmatrix}, \quad (16)$$

where \mathbf{I}_n denotes an identity matrix of dimension n and $[\mathbf{1}]_{n \times 1}$ is a column vector of dimension n with all its entries equal to 1. In addition to the state variables, two different sets of output variables are considered in this work: *interstory drifts* and *interbuilding approaches*. The interstory drifts are the relative displacements between consecutive floors of the same building, and can be defined as

$$\begin{cases} r_1^j(t) = q_1^j(t), \\ r_i^j(t) = q_i^j(t) - q_{i-1}^j(t), \quad 1 < i \leq n_j, \end{cases} \quad (17)$$

where n_j represents the number of stories of building $\mathcal{B}^{(j)}$. The vectors of interstory drifts corresponding to the buildings $\mathcal{B}^{(1)}$ and $\mathcal{B}^{(2)}$ are, respectively,

$$\mathbf{r}^{(1)}(t) = [r_1^1(t), r_2^1(t), r_3^1(t), r_4^1(t)]^T, \quad \mathbf{r}^{(2)}(t) = [r_1^2(t), r_2^2(t), r_3^2(t), r_4^2(t), r_5^2(t)]^T. \quad (18)$$

The overall vector of interstory drifts has the following form:

$$\mathbf{r}(t) = \begin{bmatrix} \mathbf{r}^{(1)}(t) \\ \mathbf{r}^{(2)}(t) \end{bmatrix} \quad (19)$$

and can be computed as

$$\mathbf{r}(t) = \mathbf{C}_r \mathbf{x}(t) \quad (20)$$

using the output matrix

$$\mathbf{C}_r = \begin{bmatrix} \tilde{\mathbf{C}}_r & [\mathbf{0}]_{9 \times 9} \end{bmatrix}, \quad (21)$$

with

$$\tilde{\mathbf{C}}_r = \begin{bmatrix} \mathbf{C}_r^{(1)} & [\mathbf{0}]_{4 \times 5} \\ [\mathbf{0}]_{5 \times 4} & \mathbf{C}_r^{(2)} \end{bmatrix}, \quad \mathbf{C}_r^{(1)} = \begin{bmatrix} 1 & 0 & 0 & 0 \\ -1 & 1 & 0 & 0 \\ 0 & -1 & 1 & 0 \\ 0 & 0 & -1 & 1 \end{bmatrix}, \quad \mathbf{C}_r^{(2)} = \begin{bmatrix} 1 & 0 & 0 & 0 & 0 \\ -1 & 1 & 0 & 0 & 0 \\ 0 & -1 & 1 & 0 & 0 \\ 0 & 0 & -1 & 1 & 0 \\ 0 & 0 & 0 & -1 & 1 \end{bmatrix}. \quad (22)$$

The interbuilding approaches describe the approaching between stories placed at the same level in adjacent buildings

$$a_i(t) = -(q_i^2(t) - q_i^1(t)), \quad 1 \leq i \leq \min(n_1, n_2). \quad (23)$$

For our particular two-building system, the vector of interbuilding approaches

$$\mathbf{a}(t) = [a_1(t), a_2(t), a_3(t), a_4(t)]^T, \quad (24)$$

can be computed as

$$\mathbf{a}(t) = \mathbf{C}_a \mathbf{x}(t), \quad (25)$$

using the output matrix

$$\mathbf{C}_a = \begin{bmatrix} \tilde{\mathbf{C}}_a & [\mathbf{0}]_{4 \times 9} \end{bmatrix}, \quad (26)$$

with

$$\tilde{\mathbf{C}}_a = [\mathbf{I}_4 \quad -\mathbf{I}_4 \quad [\mathbf{0}]_{4 \times 1}]. \quad (27)$$

3. Static output-feedback H_∞ controllers design

In order to prevent buildings' structural damage and interbuilding collisions, large interstory drifts and interbuilding approaches must both be avoided. Additionally, moderate control efforts are also convenient. To this end, we consider the vector of controlled outputs

$$\mathbf{z}(t) = \mathbf{C}_z \mathbf{x}(t) + \mathbf{D}_z \mathbf{u}(t), \quad (28)$$

with

$$\mathbf{C}_z = \begin{bmatrix} \alpha_r \tilde{\mathbf{C}}_r & [\mathbf{0}]_{9 \times 9} \\ \alpha_a \tilde{\mathbf{C}}_a & [\mathbf{0}]_{4 \times 9} \\ [\mathbf{0}]_{3 \times 9} & [\mathbf{0}]_{3 \times 9} \end{bmatrix}, \quad \mathbf{D}_z = \begin{bmatrix} [\mathbf{0}]_{13 \times 3} \\ \alpha_u \mathbf{I}_3 \end{bmatrix}, \quad (29)$$

where α_r , α_a and α_u are scaling coefficients that compensate the different magnitude of interstory drifts, interbuilding approaches and control forces, respectively. Regarding the feedback information, we assume that the relative velocities associated to the actuation devices are measurable and consider the following vector of observed outputs:

$$\mathbf{y}(t) = [y_1(t), y_2(t), y_3(t)]^T, \quad (30)$$

where $y_1(t)$ and $y_2(t)$ represent the interstory velocity at the first-story level in buildings $\mathcal{B}^{(1)}$ and $\mathcal{B}^{(2)}$, respectively, and $y_3(t)$ is the interbuilding velocity at the four-story level. The vector $\mathbf{y}(t)$ can be written as a linear combination of the states

$$\mathbf{y}(t) = \mathbf{C}_y \mathbf{x}(t) \quad (31)$$

with the observed output matrix

$$\mathbf{C}_y = \begin{bmatrix} 0 & 0 & 0 & 0 & 0 & 0 & 0 & 0 & 0 & 0 & 1 & 0 & 0 & 0 & 0 & 0 & 0 & 0 & 0 \\ 0 & 0 & 0 & 0 & 0 & 0 & 0 & 0 & 0 & 0 & 0 & 0 & 0 & 0 & 1 & 0 & 0 & 0 & 0 \\ 0 & 0 & 0 & 0 & 0 & 0 & 0 & 0 & 0 & 0 & 0 & 0 & 0 & -1 & 0 & 0 & 0 & 1 & 0 \end{bmatrix}. \quad (32)$$

According to the results presented in [16,17], a suboptimal static output-feedback H_∞ controller

$$\mathbf{u}(t) = \mathbf{K} \mathbf{y}(t) \quad (33)$$

for the first-order system in Eq.(14) and the controlled output defined in Eq.(28) can be computed by solving the following LMI optimization problem:

$$\mathcal{P} : \begin{cases} \text{maximize } \eta \\ \text{subject to } \mathbf{X}_Q > 0, \mathbf{X}_R > 0, \eta > 0 \text{ and the LMI in (35),} \end{cases} \quad (34)$$

$$\begin{bmatrix} \mathbf{A} \mathbf{Q} \mathbf{X}_Q \mathbf{Q}^T + \mathbf{Q} \mathbf{X}_Q \mathbf{Q}^T \mathbf{A}^T + \mathbf{A} \mathbf{R} \mathbf{X}_R \mathbf{R}^T + \mathbf{R} \mathbf{X}_R \mathbf{R}^T \mathbf{A}^T + \mathbf{B} \mathbf{Y}_R \mathbf{R}^T + \mathbf{R} \mathbf{Y}_R^T \mathbf{B}^T + \eta \mathbf{E} \mathbf{E}^T & * \\ \mathbf{C}_z \mathbf{Q} \mathbf{X}_Q \mathbf{Q}^T + \mathbf{C}_z \mathbf{R} \mathbf{X}_R \mathbf{R}^T + \mathbf{D}_z \mathbf{Y}_R \mathbf{R}^T & -\mathbf{I} \end{bmatrix} < 0, \quad (35)$$

where $*$ denotes the symmetric entry, \mathbf{X}_Q , \mathbf{X}_R and \mathbf{Y}_R are the optimization variables, \mathbf{Q} is a matrix whose columns contain a basis of $\text{Ker}(\mathbf{C}_y)$ and the matrix \mathbf{R} has the following form:

$$\mathbf{R} = \mathbf{C}_y^\dagger + \mathbf{Q} \tilde{\mathbf{L}}, \quad \tilde{\mathbf{L}} = \mathbf{Q}^\dagger \tilde{\mathbf{X}} \mathbf{C}_y^T (\mathbf{C}_y \tilde{\mathbf{X}} \mathbf{C}_y^T)^{-1}, \quad (36)$$

where

$$\mathbf{C}_y^\dagger = \mathbf{C}_y^T (\mathbf{C}_y \mathbf{C}_y^T)^{-1}, \quad \mathbf{Q}^\dagger = (\mathbf{Q}^T \mathbf{Q})^{-1} \mathbf{Q}^T \quad (37)$$

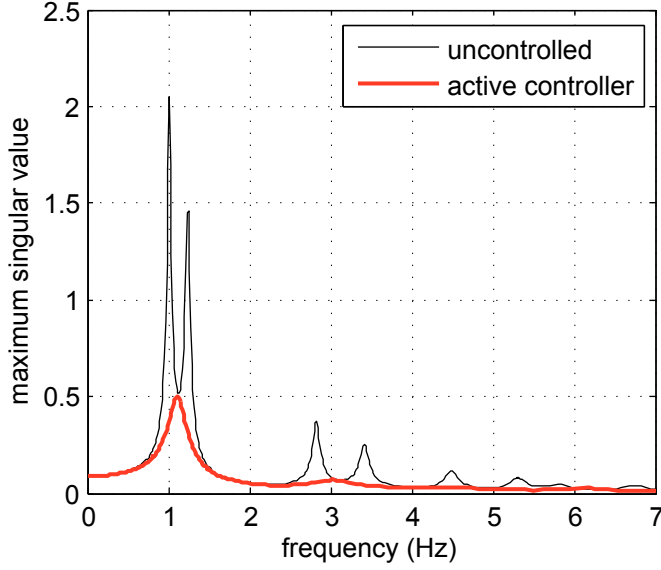


Figure 2. Frequency response corresponding to the centralized velocity-feedback H_∞ controller with active implementation defined by the control gain matrix \mathbf{K} . Maximum singular values of the closed-loop pulse transfer function $\mathbf{T}_K(2\pi f j)$ (red thick line) and the open-loop transfer function $\mathbf{T}(2\pi f j)$ (black thin line).

are the *Moore-Penrose* pseudoinverses of \mathbf{C}_y and \mathbf{Q} , respectively, and $\tilde{\mathbf{X}}$ is the optimal X -matrix of the auxiliary LMI optimization problem

$$\mathcal{P}_a : \begin{cases} \text{maximize } \eta_a \\ \text{subject to } \mathbf{X} > 0, \eta_a > 0 \text{ and the LMI in (39),} \end{cases} \quad (38)$$

$$\begin{bmatrix} \mathbf{A}\mathbf{X} + \mathbf{X}\mathbf{A}^T + \mathbf{B}\mathbf{Y} + \mathbf{Y}^T\mathbf{B}^T + \eta_a\mathbf{E}\mathbf{E}^T & * \\ \mathbf{C}_z\mathbf{X} + \mathbf{D}_z\mathbf{Y} & -\mathbf{I} \end{bmatrix} < 0. \quad (39)$$

If an optimal value $\tilde{\eta}$ is attained in \mathcal{P} for the triplet $(\tilde{\mathbf{X}}_Q, \tilde{\mathbf{X}}_R, \tilde{\mathbf{Y}}_R)$, then the output gain matrix \mathbf{K} can be written in the form

$$\mathbf{K} = \tilde{\mathbf{Y}}_R(\tilde{\mathbf{X}}_R)^{-1}. \quad (40)$$

Moreover, the inequality

$$\gamma_K \leq (\tilde{\eta})^{-1/2} \quad (41)$$

holds for the H_∞ norm

$$\gamma_K = \sup_{\|w\|_2 \neq 0} \frac{\|z\|_2}{\|w\|_2} = \sup_f \sigma_{\max}[\mathbf{T}_K(2\pi f j)], \quad (42)$$

where $j = \sqrt{-1}$, f is the frequency in hertz, $\sigma_{\max}[\cdot]$ denotes the maximum singular value and

$$\mathbf{T}_K(s) = \mathbf{C}_K(s\mathbf{I} - \mathbf{A}_K)^{-1}\mathbf{E}, \quad (43)$$

with

$$\mathbf{A}_K = \mathbf{A} + \mathbf{B}\mathbf{K}\mathbf{C}_y, \quad \mathbf{C}_K = \mathbf{C}_z + \mathbf{D}_z\mathbf{K}\mathbf{C}_y, \quad (44)$$

is the closed-loop transfer function from the disturbance input to the controlled output.

By applying the described computational procedure with the system matrices \mathbf{A} , \mathbf{B} and \mathbf{E} in Eqs. (15) and (16), corresponding to the mass and stiffness values given in Table 1 and the damping matrices in Eqs. (11) and (12); the observed output matrix \mathbf{C}_y in Eq. (32); and the controlled output matrices \mathbf{C}_z and \mathbf{D}_z in Eq. (29), defined by the scaling coefficients

$$\alpha_r = 5, \quad \alpha_a = 1, \quad \alpha_u = 10^{-7.4}, \quad (45)$$

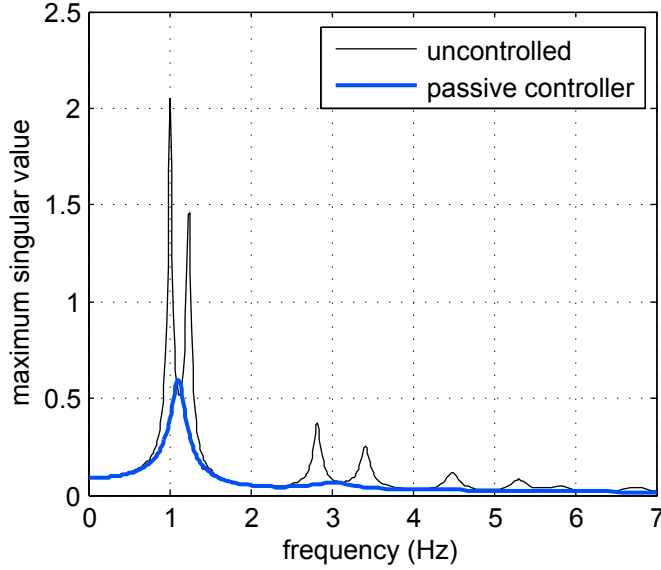


Figure 3. Frequency response corresponding to the decentralized velocity-feedback H_∞ with passive implementation defined by the control gain matrix $\hat{\mathbf{K}}$. Maximum singular values of the closed-loop pulse transfer function $\mathbf{T}_{\hat{\mathbf{K}}}(2\pi f j)$ (blue thick line) and the open-loop transfer function $\mathbf{T}(2\pi f j)$ (black thin line).

we obtain the following output-feedback control gain matrix:

$$\mathbf{K} = 10^6 \times \begin{bmatrix} -6.7995 & -3.7537 & -0.3298 \\ -1.2424 & -8.6100 & 0.3551 \\ 0.5163 & 0.9621 & -2.9368 \end{bmatrix}, \quad (46)$$

and the γ -value upper bound

$$\gamma_{\mathbf{K}} \leq 0.6529. \quad (47)$$

By computing the peak-value of the maximum singular values corresponding to the pulse transfer function $\mathbf{T}_{\mathbf{K}}(2\pi f j)$, we find that the actual γ -value is

$$\gamma_{\mathbf{K}} = 0.5034. \quad (48)$$

The particular values of the scaling coefficients α_r , α_a and α_u in Eq. (45) have been selected by considering the peak-value magnitude of interstory drifts, interbuilding approaches and control forces, which are in the order of 10^{-2}m , 10^{-1}m and 10^6N , respectively (see the plots in Figure 5, Figure 6, Figure 7 and the values in Table 2).

To illustrate the frequency behavior of the output-feedback controller defined by the gain matrix \mathbf{K} , the maximum singular values of the closed-loop pulse transfer function $\mathbf{T}_{\mathbf{K}}(2\pi f j)$ and the open-loop pulse transfer function

$$\mathbf{T}(2\pi f j) = \mathbf{C}_z(2\pi f j \mathbf{I} - \mathbf{A})^{-1} \mathbf{E} \quad (49)$$

are presented in Figure 2. In this figure, the black thin line displays the open-loop transfer function and shows the frequency response characteristics of the uncontrolled structure. The peaks in this plot are associated to the resonant frequencies of the individual buildings, which are located at 1.24 Hz, 3.42 Hz, 5.32 Hz and 6.72 Hz for building $\mathcal{B}^{(1)}$ and at 1.01 Hz, 2.82 Hz, 4.49 Hz, 5.80 Hz and 6.77 Hz for building $\mathcal{B}^{(2)}$. The red thick line, corresponding to the closed-loop transfer function $\mathbf{T}_{\mathbf{K}}(2\pi f j)$, presents a single relevant peak of magnitude $\gamma_{\mathbf{K}} = 0.5034$ located between the two main resonant modes and clearly shows the positive effect of the proposed output-feedback H_∞ controller.

From a practical point of view, the controller defined by the output-feedback gain matrix \mathbf{K} in Eq. (46) has the important advantage of using a reduced system of sensors which are

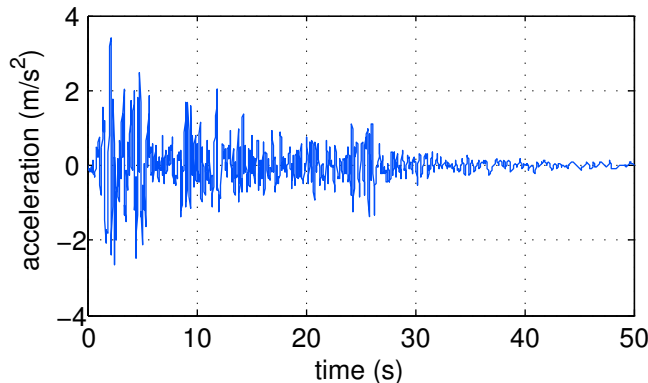


Figure 4. Full scale North–South El Centro 1940 seismic record.

naturally associated to the actuation devices. However, it also presents two serious drawbacks. Firstly, the complete vector of observed outputs is used to compute the control actions and, consequently, a wide communication system would be necessary in the controller implementation. Secondly, producing the corresponding actuation forces would require active devices with a large power consumption and potential reliability issues. These two disadvantages, typically present in vibration control of large structures, can be properly overcome by considering a fully decentralized velocity-feedback controller. By solving the LMI optimization problem \mathcal{P} in Eq. (34) with the same matrices used in the previous controller design and constraining the LMI variable matrices \mathbf{X}_R and \mathbf{Y}_R to a diagonal form, we obtain the following decentralized output-feedback control gain matrix:

$$\hat{\mathbf{K}} = 10^6 \times \begin{bmatrix} -6.1629 & 0 & 0 \\ 0 & -9.2165 & 0 \\ 0 & 0 & -3.2567 \end{bmatrix}, \quad (50)$$

and the γ -value upper bound

$$\gamma_{\hat{\mathbf{K}}} \leq 0.7648. \quad (51)$$

By computing the peak of the maximum singular values corresponding to the pulse transfer function $\mathbf{T}_{\hat{\mathbf{K}}}(2\pi f j)$, we find the γ -value

$$\gamma_{\hat{\mathbf{K}}} = 0.5980. \quad (52)$$

As indicated in [13,18], the control actions associated to the fully decentralized velocity-feedback controller

$$\mathbf{u}(t) = \hat{\mathbf{K}}\mathbf{y}(t) \quad (53)$$

can be implemented using two passive interstory actuation devices d_1 and d_2 with respective damping constants 6.1629 MNs/m and 9.2165 MNs/m, and a passive interbuilding actuator with damping constant 3.2567 MNs/m. The frequency response characteristics of this second controller are displayed in Figure 3, where the blue thick line corresponds to the closed-loop transfer function $\mathbf{T}_{\hat{\mathbf{K}}}(2\pi f j)$ and the black thin line represents the open-loop transfer function.

4. Numerical simulations

In this section, numerical simulations are conducted to investigate the seismic vibrational response of the considered two-building system for three different control configurations: (i) *Uncontrolled*. No control system is implemented. (ii) *Active controller*. The control system includes three ideal active devices, which are driven by the output-feedback controller defined by the control gain matrix \mathbf{K} in Eq. (46). (iii) *Passive controller*. The control system includes

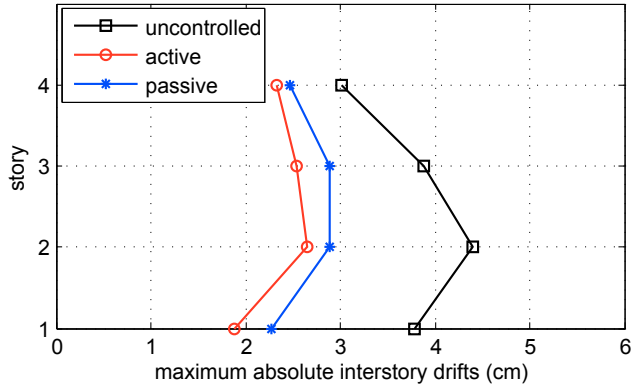


Figure 5. Maximum absolute interstory drifts in building $\mathcal{B}^{(1)}$ corresponding to the uncontrolled configuration (black line with squares), the active controller defined by the control gain matrix \mathbf{K} (red line with circles) and the passive controller defined by the control gain matrix $\hat{\mathbf{K}}$ (blue line with asterisks).

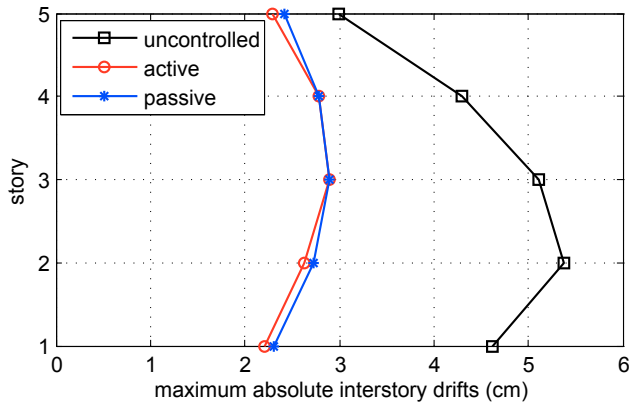


Figure 6. Maximum absolute interstory drifts in building $\mathcal{B}^{(2)}$ corresponding to the uncontrolled configuration (black line with squares), the active controller defined by the control gain matrix \mathbf{K} (red line with circles) and the passive controller defined by the control gain matrix $\hat{\mathbf{K}}$ (blue line with asterisks).

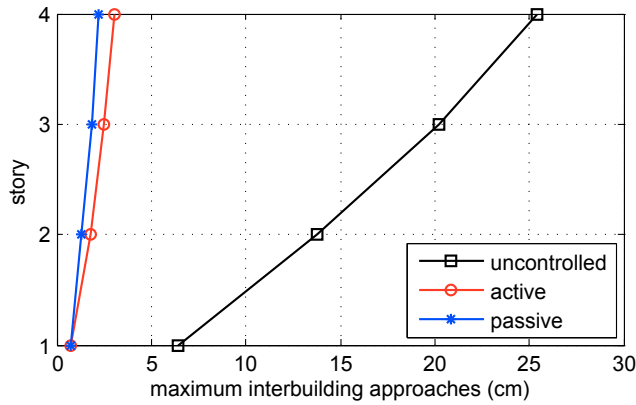


Figure 7. Maximum interbuilding approaches corresponding to the uncontrolled configuration (black line with squares), the active controller defined by the control gain matrix \mathbf{K} (red line with circles) and the passive controller defined by the control gain matrix $\hat{\mathbf{K}}$ (blue line with asterisks).

three linear passive dampers with the damping capacities defined by the diagonal elements of the decentralized control gain matrix $\hat{\mathbf{K}}$ in Eq. (50). In all the cases, the full scale *North-South El Centro 1940* seismic record is taken as ground acceleration disturbance (see Figure 4), and the interbuilding approaches $\mathbf{a}(t)$ together with the interstory drifts $\mathbf{r}(t)$ are computed as output variables. In the controlled cases, the vector of control efforts $\mathbf{u}(t)$ is also computed. In order to avoid modeling and simulation difficulties associated to interbuilding collisions, the interbuilding gap is assumed to be large enough to prevent pounding events, and the maximum interbuilding approaches are understood as lower bounds of safe interbuilding distances.

To gain an overall insight into the behavior of the proposed controllers, the maximum values of the absolute interstory drifts corresponding to the buildings $\mathcal{B}^{(1)}$ and $\mathcal{B}^{(2)}$ are presented in Figure 5 and Figure 6, respectively, and the maximum interbuilding approaches are displayed

Table 2. Maximum absolute control efforts ($\times 10^6$ N)

Actuation device	d_1	d_2	d_3
Active controller	1.4755	1.6157	0.6366
Passive controller	1.0576	1.6425	0.6391

in Figure 7. In these figures, the black line with squares corresponds to the uncontrolled configuration, the red line with circles shows the response of the active controller defined by the control gain matrix \mathbf{K} , and the blue line with asterisks presents the behavior of the passive controller defined by the control gain matrix $\hat{\mathbf{K}}$.

A quick inspection of the graphics in Figure 5 and Figure 6 shows that the proposed controllers provide a good level of reduction in the buildings' interstory-drift peak-values. In building $\mathcal{B}^{(1)}$ (see Figure 5), the uncontrolled configuration produces a maximum absolute interstory-drift peak-value of about 4.4 cm, while the maximum peak-values corresponding to the controlled configurations remain below 3.0 cm. In building $\mathcal{B}^{(2)}$ (see Figure 6), the maximum interstory-drift peak-value produced by the uncontrolled configuration is 5.4 cm and the maximum peak-values attained by the controlled configurations also remain below 3.0 cm. In relative terms, the reductions in the maximum interstory-drift peak-value in $\mathcal{B}^{(1)}$ and $\mathcal{B}^{(2)}$ are superior to 34% and 45%, respectively. Regarding the interbuilding seismic response, the plots in Figure 7 clearly indicate that the proposed controllers provide an outstanding level of protection against pounding events. In particular, an interbuilding distance of 3.5 cm can be considered safe for the controlled configurations while, in contrast, an interbuilding separation of 25 cm would produce an interbuilding collision for the uncontrolled configuration. In this case, the relative reduction attained in the maximum interbuilding-approach peak-value is of about 90%. Finally, the data collected in Table 2 indicate that the control-effort peak-values required by the proposed controllers are very similar in the case of the actuation devices d_2 and d_3 . For the actuator d_1 , the active controller demands a slightly larger control-effort peak-value, which is consistent with the better behavior exhibited by this controller in Figure 5.

5. Conclusions and future directions

In this paper, an advanced control design strategy for the seismic protection of adjacent buildings has been presented. The proposed design methodology is based on a linear matrix inequality formulation, allows including active and passive actuation devices, and makes it possible to deal with important information constraints associated to the problem. The main ideas have been illustrated by means of a two-building structure equipped with an interbuilding actuation device installed at the top level of the lowest building and two interstory actuation devices implemented at the ground level of the buildings. For this control setup, two static output-feedback H_∞ controllers have been designed: (i) a centralized velocity-feedback active controller and (ii) a fully decentralized velocity-feedback controller, which can be implemented using passive linear dampers. Numerical simulations indicate that the proposed controllers have the ability of both mitigating the buildings' structural response and providing a suitable protection against interbuilding impacts. The positive results obtained in this preliminary study indicate that further research effort should be invested in extending the proposed controller design methodology to control setups with more complex actuation systems.

Acknowledgments

This work was partially supported by the Spanish Ministry of Economy and Competitiveness under Grant DPI2015-64170-R.

References

- [1] Chau KT, Wei XX, Guo X and Shen CY 2003 Experimental and theoretical simulations of seismic poundings between two adjacent structures *Earthq. Eng. Struct. D.* **32** 537–54
- [2] Komodromos P, Polycarpou PC, Papaloizou L and Phocas MC 2007 Response of seismically isolated buildings considering poundings *Earthq. Eng. Struct. D.* **36** 1605–22
- [3] Polycarpou PC and Komodromos P 2010 Earthquake-induced poundings of a seismically isolated building with adjacent structures *Eng. Struct.* **32** 1937–51
- [4] Ying ZG, Ni YQ and Ko JM 2003 Stochastic optimal coupling-control of adjacent building structures *Comput. Struct.* **81** 2775–87
- [5] Bhaskararao AV and Jangid RS 2006 Seismic response of adjacent buildings connected with friction dampers *B. Earthq. Eng.* **4** 43–64
- [6] Kim J, Ryu J and Chung L 2006 Seismic performance of structures connected by viscoelastic dampers *Eng. Struct.* **28** 183–95
- [7] Basili M and Angelis MD 2007 Optimal passive control of adjacent structures interconnected with nonlinear hysteretic devices *J. Sound Vib.* **301** 106–25
- [8] Christenson RE, Spencer BF and Johnson EA 2007 Semiactive connected control method for adjacent multidegree-of-freedom buildings *J. Eng. Mech.* **133** 290–98
- [9] Bharti SD, Dumne SM and Shriali MK 2010 Seismic response analysis of adjacent buildings connected with MR dampers *Eng. Struct.* **32** 2122–33
- [10] Zhu HP, Ge DD and Huang X 2011 Optimum connecting dampers to reduce the seismic responses of parallel structures *J. Sound Vib.* **330** 1931–49
- [11] Palacios-Quiñonero F, Rubió-Massegú J, Rossell JM and Karimi HR 2012 Semiactive-passive structural vibration control strategy for adjacent structures under seismic excitation *J. Frankl. Inst.* **349** 3003–26
- [12] Palacios-Quiñonero F, Rossell JM, Rubió-Massegú J and Karimi HR 2012 Structural vibration control for a class of connected multistrukture mechanical systems *Math. Probl. Eng.* **2012** 1–23
- [13] Palacios-Quiñonero F, Rubió-Massegú J, Rossell JM and Karimi HR 2014 Vibration control for adjacent structures using local state information *Mechatronics* **24** 336–44
- [14] Chopra AK 2007 *Dynamics of Structures. Theory and Applications to Earthquake Engineering 3rd ed* (Upper Saddle River, NJ: Prentice Hall)
- [15] Kurata N, Kobori T, Takahashi M, Niwa N and Midorikawa H 1999 Actual seismic response controlled building with semi-active damper system *Earthq. Eng. Struct. D.* **28** 1427–47
- [16] Rubió-Massegú J, Rossell JM, Karimi HR and Palacios-Quiñonero F 2013 Static output-feedback control under information structure constraints *Automatica* **49** 313–16
- [17] Palacios-Quiñonero F, Rubió-Massegú J, Rossell JM and Karimi HR 2014 Feasibility issues in static output-feedback controller design with application to structural vibration control *J. Frankl. Inst.* **351** 139–55
- [18] Palacios-Quiñonero F, Rubió-Massegú J, Rossell JM and Karimi HR 2012 Optimal passive-damping design using a decentralized velocity-feedback H_∞ approach *Model. Ident. Control* **33** 87–97